Integrated mechano-optical hydrogen gas sensor using cantilever bending readout with a Si_3N_4 grated waveguide

So V. Pham,[1,*] Meindert Dijkstra,[1] Henk A. G. M. van Wolferen,[2] Markus Pollnau,[1] Gijs J. M. Krijnen,[2] and Hugo J. W. M. Hoekstra[1]

[1]*Integrated Optical MicroSystems (IOMS) Group, University of Twente P.O. Box 217, 7500 AE Enschede, The Netherlands*

[2]*Transducers Science and Technology (TST) Group MESA Institute for Nanotechnology, University of Twente P.O. Box 217, 7500 AE Enschede, The Netherlands*

**Corresponding author: s.v.pham@ewi.utwente.nl*

Received June 2, 2011; accepted June 25, 2011;
posted June 27, 2011 (Doc. ID 148646); published August 1, 2011

We demonstrate a proof of concept of a novel and compact integrated mechano-optical sensor for H_2 detection based on a microcantilever suspended above a Si_3N_4 grated waveguide. The fabricated devices are mechanically and optically modeled and characterized. Sensing operation of the sensor is demonstrated with 1% H_2 in N_2. The error in detection of the cantilever bending induced by absorption of H_2 is estimated to be approximately 10 nm. Significantly improved sensitivity (down to ~33 pm) is expected for reduced initial bending of the microcantilever. The simulation and experimental results are in good agreement and provide a good guideline for further optimization of the sensor. © 2011 Optical Society of America

OCIS codes: 230.4685, 130.3120, 130.6010.

A sensor is a device that can recognize the presence of a specific stimulus and translate it into a measurable signal [1]. Microcantilever-based sensors, which have effectively been exploited for biological, chemical, and gas sensing applications, can be operated in either dynamic mode by monitoring the resonant frequency of the cantilever (CL), or static mode by measuring its stress-induced deflection, as the target binds to the functionalized surface of the CL [2]. The deflection of the CL can be determined by means of bulky deflection of an optical beam [3] or electrical, i.e., capacitive, piezoresistive, or piezoelectric readouts [4–6]. Alternatively, a fully integrated optical readout with a CL waveguide was first presented in 2006 by Zinoviev *et al.* [7] and in the following 3 years by other groups [8–10]. In 2008, we proposed a novel integrated optical readout of a singly clamped CL (sCL) bending with a grated-waveguide (GWG) optical cavity and presented preliminary simulation results [11]. Recently, such integrated mechano-optical GWG-sCL devices have been fabricated and demonstrated as a proof of concept of the readout [12].

In this study, we aim at applying the proposed integrated mechano-optical readout to hydrogen gas sensing. For this purpose, a 30 nm thick palladium (Pd) receptor layer was sputtered onto the entire surface of the SiO_2 CL. At room temperature and atmospheric pressure, Pd can absorb up to 900 times its own volume of hydrogen [13]. Absorption of H_2 by Pd causes the CL, suspended above the GWG, to curl down [3–12], which narrows the GWG-CL gap, g, and leads to a stronger interaction between the CL and the GWG evanescent modal field, which results in a redshift of the transmission spectrum.

Functionalizing the SiO_2 CL by depositing the absorptive Pd film onto it causes an initial bending of the bilayer CL due to differences in their residual stresses [12]. In the fabrication batch presented in Ref. [12], an oxygen–plasma treatment was strategically applied as a means to reduce such an initial bending of the bilayer sCL. As a side effect, the Pd film was oxidized and no longer able to bind H_2. Therefore, a solution to achieve a low initial bending of the CL without deactivating the functionality of the Pd film is required. One of our proposed solutions consisted of using devices with a doubly clamped CL—a so-called bridge—in addition to the sCLs as mentioned in Ref. [12].

A three-dimensional (3D) schematic of the structure and the cross section of the GWG-microbridge device are shown in Figs. 1(a) and 1(b). All relevant device dimensions remain the same as in Ref. [12], except that here we choose an aimed gap of $g_o = 200$ nm and a bridge length of $L_b = 65\,\mu$m. A polydimethylsiloxane (PDMS) chamber was placed on top of the device and connected to gas bottles with pure N_2 and a 1% H_2–N_2 mixture through mass flow controllers. The optical performance of the integrated device was monitored using a tunable laser source (Agilent 8164B) with a resolution of 1 pm and an InGaAs photodetector.

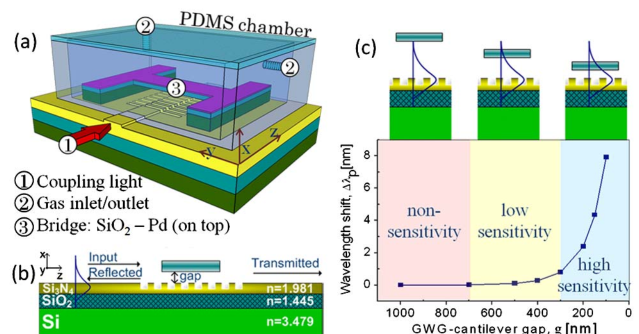

Fig. 1. (Color online) (a) 3D schematic of the structure with a PDMS chamber serving as a reaction environment for H_2 sensing, (b) cross section of the GWG-CL device, and (c) simulated resonant wavelength shift for various gap sizes, illustrating three operating regions of the sensor.

0146-9592/11/153003-03$15.00/0 © 2011 Optical Society of America

Response of the sensor with different gaps was simulated using the bidirectional eigenmode propagation method, as shown in Fig. 1(c) [11]. The results indicate three sensitivity regions of the sensor, depending on the overlap of the CL with the evanescent tail of the GWG modes.

Initial bending δ_{0c} of the tip of the singly clamped bilayer CLs was predicted using the Timoshenko formulas [14–16] described in Eq. (1), considering the dimensions and material properties [17] of the CLs summarized in Table 1:

$$\delta_{0c} = L_c^2 \times \frac{3w_1 w_2 E_1 E_2 t_1 t_2 (t_1 + t_2)\left[\left(\frac{\sigma_{02}}{E_2} - \frac{\sigma_{01}}{E_1}\right) + (\alpha_2 - \alpha_1)\Delta T\right]}{(w_1 E_1 t_1^2)^2 + (w_2 E_2 t_2^2)^2 + 2w_1 w_2 E_1 E_2 t_1 t_2 (2t_1^2 + 3t_1 t_2 + 2t_2^2)}, \quad (1)$$

where δ_0, L, w_i, and t_i are the initial bending, length, width, and thickness of the CLs; E_i, σ_{0i}, and α_i are Young's modulus, the residual stress and thermal expansion coefficient of material i, with the subscripts $i = 1$ and 2 representing the SiO_2 and Pd layers, respectively. The residual stresses of the films were determined based on Stoney's formula $\sigma_0 = E_s t^2 / [6R(1 - \upsilon_s)]$, where E_s and υ_s are Young's modulus and the Poisson ratio of the substrate, and R is the radius of curvature, obtained by measuring the wafer curvature, $1/R$, due to deposition of the film on a silicon substrate [1]; their values are $\sigma_{01} \sim -310$ MPa (compressive stress) and $\sigma_{02} \sim 1000$ MPa (tensile stress) for SiO_2 and Pd films, respectively.

The residual stress acting on the bilayer CLs is equivalent to an accumulated force F_0 acting on the tip of the sCL or at the middle of the bridge and, thus, the initial deflections of the CLs $(\delta_{0c}, \delta_{0b})$ are alternatively expressed as Eqs. (2) and (3) below [16]. Therefore, once the initial bending of the sCL, δ_{0c}, was calculated by Eq. (1), the initial bending of the middle of the bridge, δ_{0b}, was then deduced using Eq. (4):

$$\delta_{0c} = \frac{F_0 L_c^3}{3\mathrm{EI}}, \quad (2)$$

$$\delta_{0b} = \frac{F_0 L_b^3}{192\mathrm{EI}}, \quad (3)$$

$$\delta_{0b} \sim \left(\frac{L_b}{4L_c}\right)^3 \delta_{0c}, \quad (4)$$

Table 1. Dimensions and Material Properties of the CLs

Materials	SiO_2 (1)	Pd (2)
Length L_c (μm)	30	30
Width w (μm)	20	20
Thickness t (μm)	0.8	0.03
Young modulus E (GPa)	61	121
Residual stress σ_0 (MPa)	–310	1000
Thermal expansion coefficient α (10^{-6}/K)	0.55	11.6

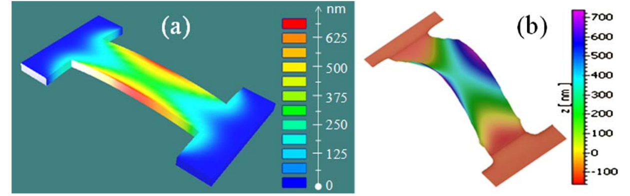

Fig. 2. (Color online) Initial bending of the bridge due to differences in residual stress of the films. (a) Numerical simulation using INTELLISUITE software package, (b) experimental result attained by a white-light interferometer, showing an initial upbending of ~500 nm at the center of the microbridge.

with $I = wt^3/12$, the moment of inertia of the CLs having a rectangular cross section.

For comparison, finite-element simulations of the CLs were carried out using the INTELLISUITE software package [17], as shown in Fig. 2(a) (only the bridge structure is shown here). The initial bending of the fabricated sCL and bridge was characterized using a white-light interferometer. Figure 2(b) shows a 3D image of the fabricated bridge, as recorded with a white-light interferometer, indicating an initial bending (upwards, i.e., away from the GWG structure) of approximately 500 nm. The analytically calculated, numerically simulated, and experimentally measured values of the initial deflections are in good agreement and summarized in Table 2. The table also shows the resulting gap, $g = g_0 + \delta_0$, of the GWG-sCL/bridge devices. The GWG-sCL device is not suitable for H_2 sensing, because the gap $g \sim 3155$ nm is in the insensitive region of the sensor. On the contrary, the GWG-bridge device is able to detect H_2, even though the gap $g \sim 700$ nm is in the low-sensitivity region of the sensor, as predicted in Fig. 1(c). This initial bending leads to a lower sensitivity at low H_2 concentrations.

Prior to supplying H_2 gas to the measurement chamber, N_2 gas was flushed in during 15 min with a flow rate of 0.5 sccm and optical transmission curves were captured repeatedly every minute. The results showed a stable and reproducible resonant peak at $\lambda_p = 1496.631 \pm 0.001$ nm [see Fig. 3(a), curve at $t = 0$], indicating that such a flow rate did not cause any side effects or mechano-optical vibrations. Noise was removed from the spectrum using low-pass filtering in the Fourier domain, enabling accurate and efficient determination of changes in $\Delta\lambda_p = \lambda_p(t) - \lambda_p(t_o)$.

Next we supplied the H_2(1%)–N_2 mixture at a flow rate of 0.5 sccm for a longer period of time, during which the transmission spectrum was monitored [see Fig. 3(a)]. The shift $\Delta\lambda_p$ depends almost linearly on time [Fig. 3(b), left-hand side), which can be explained partly by noting

Table 2. Initial Bending δ_0 of the CLs and the Final Fabricated Gap $g = g_0 + \delta_0$, and Sensitivity for Thermal Drift $\Delta\delta/\Delta T$

	sCL	Bridge
Length (μm)	30	65
Calculated δ_0 (nm)	2977	473
Simulated δ_0 (nm)	3196	~510
Measured δ_0 (nm)	~2955	~500
Final fabricated gap g (nm)	~3155	~700
Calculated $\Delta\delta/\Delta T$ (nm/K)	~2.5	~0.4

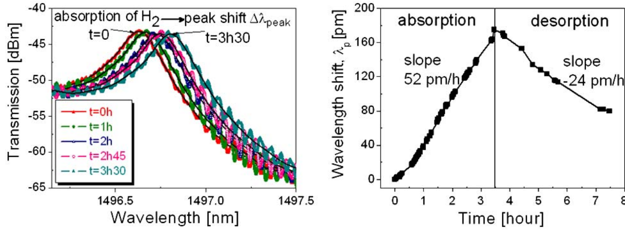

Fig. 3. (Color online) (a) Transmission curves of the device in response to the absorption (filtered and unfiltered curves) and (b) the amount of wavelength shift $\Delta\lambda_p$ versus the reaction time. Absorption (left-hand side) and desorption (right-hand side).

that the effect of the initially rapid change of the gap size, g, is compensated by lower values of $\partial\lambda_p/\partial g$ at larger gap size. After 3.5 h the flow of the H_2(1%)–N_2 mixture was switched off and replaced again by a pure N_2 flow, leading to desorption. Figure 3(b) (right-hand side) shows the resulting peak shifts during a 4 h period. It can be concluded that the desorption takes place at a much lower rate of ~50% than the absorption process, and full desorption is not achieved during the monitoring period of time.

The result provides a proof of concept of a novel and compact integrated mechano-optical sensor, which underlines the feasibility of this type of sensor.

In practice, operation of the sensor is also affected by environmental changes due to the fluctuations in temperature, ΔT. The difference in the thermal expansion coefficients between Pd and SiO_2 causes a deflection change of ~2.5 nm/K for the sCL and ~0.4 nm/K for the bridge, which is theoretically estimated by omitting the quantity $\sigma_{02}/E_2 - \sigma_{01}/E_1$ and retaining the quantity $(\alpha_2 - \alpha_1)\Delta T$ in Eq. (1) with the parameters listed in Table 1. In addition, a temperature change also leads to a spectral shift of the grated-waveguide readout. The resonant wavelength peak due to the temperature variation is measured, as shown in Fig. 4. The result shows a linear relationship $\lambda_p(T)$ with a slope $\Delta\lambda_p/\Delta T = 16$ pm/K.

We have demonstrated H_2 sensing with a novel and compact integrated optical readout scheme as a proof of concept for our mechano-optical sensor. It was found that the error in the peak shift, owing to noise and thermal fluctuations in the temperature-stabilized setup, is around 1 pm. Then, using that $\Delta\lambda_p/\Delta g = 0.1$, 0.8, and 30 pm/nm, at a gap of $g = 700$, 500, and 200 nm, respectively [according to the theoretical curve in Fig. 1(c)], the error in detection of the gap is given by 10 nm, 1.25 nm, and 33 pm for the aforementioned gap sizes, respectively. This new sensor type possesses a great potential as an element of a sensitive, on-chip multisensing system, provided that the gap between the GWG and the microcantilever, i.e., sCL and bridge, can be well controlled during fabrication. The sensing principle presented here could also be used for other specific surface reactions in a gaseous environment. For use in a liquid environment, e.g., label-free protein sensing exploiting an antigen–antibody reaction on the CL surface, the stiction problem between CL and GWG caused by adhesive forces must be solved.

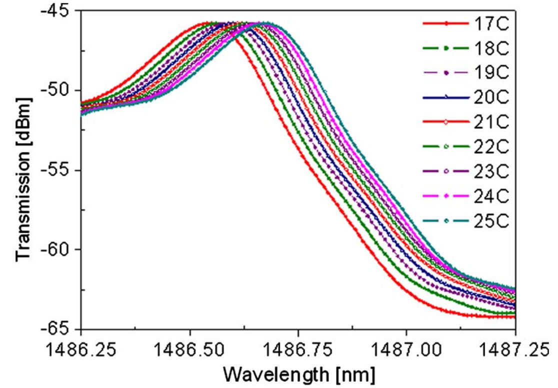

Fig. 4. (Color online) Temperature dependence of the integrated optical readout; the change of resonant wavelength shift is 16 pm/K.

This research was supported by MEMSland, a project of the Point One program funded by the Dutch Ministry of Economic Affairs and the Dutch Technology Foundation —STW through project TOE 6596. The authors thank L. J. Kauppinen and R. M. de Ridder for fruitful discussions and A. J. F. Hollink for technical support.

References

1. M. J. Madou, *Fundamentals of Microfabrication: The Science of Miniaturization*, 2nd ed., (CRC Press, 2002).
2. M. Alvarez and L. M. Lechuga, Analyst **135**, 827 (2010).
3. S. Okuyama, Y. Mitobe, K. Okuyama, and K. Matsushita, Jpn. J. Appl. Phys. **39**, 3584 (2000).
4. D. R. Baselt, B. Fruhberger, E. Klaassen, S. Cemalovic, C. L. Britton Jr., S. V. Patel, T. E. Mlsna, D. McCorkle, and B. Warmack, Sens. Actuators B Chem. **88**, 120 (2003).
5. Z. Hu, T. Thundat, and R. J. Warmack, J. Appl. Phys. **90**, 427 (2001).
6. A. Loui, F. T. Goericke, T. V. Ratto, J. Lee, B. R. Hart, and W. P. King, Sens. Actuators A Phys. **147**, 516 (2008).
7. K. Zinoviev, C. Dominguez, J. A. Plaza, V. J. C. Busto, and L. M. Lechuga, J. Lightwave Technol. **24**, 2132 (2006).
8. M. Nordstrom, D. A. Zauner, M. Calleja, J. Hubner, and A. Boisen, Appl. Phys. Lett. **91**, 103512 (2007).
9. J. W. Noh, R. Anderson, S. Kim, J. Cardenas, and G. Nordin, Opt. Express **16**, 12114 (2008).
10. S. T. Koev, R. Fernandes, W. E. Bentley, and R. Ghodssi, IEEE Trans. Biomed. Circuits Syst. **3**, 415 (2009).
11. L. J. Kauppinen, H. J. W. M. Hoekstra, M. Dijkstra, R. M. de Ridder, and G. J. M. Krijnen, *Proceedings of the 14th European Conference on Integrated Optics* (Eindhoven University of Technology, 2008), pp. 111–114.
12. S. V. Pham, L. J. Kauppinen, M. Dijkstra, H. A. G. M. van Wolferen, R. M. de Ridder, and H. J. W. M. Hoekstra, IEEE Photon. Technol. Lett. **23**, 215 (2011).
13. Z. H. Chen, J. S. Jie, L. B. Luo, H. Wang, C. S. Lee, and S. T. Lee, Nanotech. Precis. Eng. **18**, 345502 (2007).
14. M. D. Nguyen, H. Nazeer, K. Karakaya, S. V. Pham, R. Steenwelle, M. Dekkers, L. Abelmann, D. H. A. Blank, and G. Rijnders, J. Micromech. Microeng. **20**, 085022 (2010).
15. M. Calleja, J. Tamayo, M. Nordström, and A. Boisen, Appl. Phys. Lett. **88**, 113901 (2006).
16. J. M. Gere and S. P. Timoshenko, *Mechanics of Materials*, 4th SI ed. (Stanley Thornes, 1999).
17. Intellisuite software, http://www.intellisense.com/.